



Influence of Cu content on microstructure, grain orientation and mechanical properties of Sn–*x*Cu lead-free solders

Kannachai KANLAYASIRI¹, Niwat MOOKAM²

1. Department of Industrial Engineering, School of Engineering,

King Mongkut's Institute of Technology Ladkrabang, Bangkok 10520, Thailand;

2. Department of Industrial and Production Engineering, Faculty of Industry and Technology,

Rajamangala University of Technology Rattanakosin Wang Klai Kangwon Campus,

Prachuapkhirikhan 77110, Thailand

Received 20 April 2021; accepted 17 November 2021

Abstract: The effect of Cu content on the microstructure, grain orientation and mechanical properties of Sn–*x*Cu (*x*=0–4.0 wt.%) lead-free solder was studied. Results showed that added Cu induced the formation of intermetallic phases. Only the η -Cu₆Sn₅ and ε -Cu₃Sn phases were present in the β -Sn matrix. For all contents, the strongly preferred orientation of the β -Sn phase was formed on the {001} plane. In Sn doped with 1.0 wt.% Cu, the η -Cu₆Sn₅ phase exhibited the preferred orientation of {0001} plane, whereas doping with 3.0 or 4.0 wt.% Cu transformed the preferred orientation to the {010} plane. In addition, only the {0001} and {10 $\bar{1}$ 0} planes were present in the ε -Cu₃Sn phase. The high Cu contents contributed to an increased number of low-angle boundaries, high residual strain, tensile strength and microhardness.

Key words: lead-free solder; Sn–Cu alloys; crystallographic orientation; microstructure; intermetallics; mechanical properties

1 Introduction

Sn–Pb eutectic solder has been extensively used in electronic industries, because of its low melting temperature, solderability, low cost and reasonable electrical conductivity [1,2]. Unfortunately, the toxicity of Pb raises serious environmental and health concerns [3]. When the Restriction of Hazardous Substances Directive, or RoHS, became effective on the 1st July 2006, the law forbade the use of Pb–Sn alloys and dictated a safe substitute for Pb-containing solder [4,5].

Of the replacements, Sn-based binary alloys are improved by doping with various elements, e.g. Ag, Sb, Bi, Ni and Cu. However, adding these elements alters the microstructure and other

properties. The drawback and improvement of some of those solders were described by OSÓRIO et al [6], who studied Sn–2.0Ag and Sn–3.5Ag alloys. The microstructures of both solders were characterized by the primary β -Sn phase with a eutectic mixture (Ag₃Sn and β -Sn phase). The tensile strength increased with more Ag₃Sn particles, but the high Ag content reduced ductility. Sn–Sb systems had the best microstructure, combining both strength and ductility for the Sn–2.0Sb alloy, due to very fine β -Sn dendrites reinforced by fine structure of the Sn–Sb layers [7]. Added Bi in the solder also improved tensile strength, due to increase in the β -Sn and eutectic area in the solder matrix [8]. HOU et al [9] studied eutectic growth in the Sn–*x*Ni systems (*x*=0.04–0.26 wt.%), the competition between stable Sn–Ni₃Sn₄ and

metastable Sn–NiSn₄ eutectic growth was studied during solidification. Sn was shown to have a good lattice match between β -Sn and NiSn₄ phase, and no preferred orientation relationship was measured between Ni₃Sn₄ and β -Sn. Thus, the addition of some elements into the pure Sn matrix promoted the formation of the intermetallic phases and affected the β -Sn phase and its mechanical properties. Large β -Sn grain size has major effects on overall solder performance and reliability, because fine grains and multiple orientations improved the thermomechanical properties [10].

In Sn–Cu systems, the η -Cu₆Sn₅, η' -Cu₆Sn₅, and ε -Cu₃Sn phases are common intermetallic phases in solder. ZENG et al [11] reported that a great number of proeutectic β -Sn dendrites formed and the η -Cu₆Sn₅ existed mostly among the proeutectic β -Sn phases in the Sn– x Cu with low Cu content, specifically, 0.3, 0.6, 1.3 and 1.7 wt.% Cu. However, MADENI et al [12] found that the microstructural constituents were dendrites of β -Sn and the eutectic interdendritic constituent consisted of the η -Cu₆Sn₅ phase in the Sn–0.7Cu alloy. Slower cooling rates led to larger dendritic microstructures. Thus, the occurrence of dendritic formation was dependent on the eutectic formation. VENTURA et al [13] found that Sn–Cu was a weakly irregular eutectic system with η -Cu₆Sn₅, leading the eutectic structure. In the Sn–0.5Cu alloy, primary β -Sn dendrites were surrounded by a fine eutectic structure. Increasing the Cu content to 0.7 wt.% leads to a more β -Sn dendritic morphology. However, increasing to 0.9 wt.% Cu, did not lead to any more primary β -Sn dendrites and the microstructure was made of a fine eutectic, with η -Cu₆Sn₅ fibres surrounded by the β -Sn matrix.

On the other hand, under an equilibrium solidification, with slow cooling, Sn–0.7Cu alloys showed equilibrium eutectic and Sn–1.0Cu alloys showed hypereutectic reactions. With rapid cooling, strong kinetic undercooling led to the eutectic point shifting to a higher Cu content. In addition, the formation of β -Sn dendrites and the intermetallic phase was controlled by mismatched crystalline orientation relationships [14]. In Sn–2.0Cu and Sn–4.0Cu hypereutectic alloys, η -Cu₆Sn₅ was surrounded by a eutectic β -Sn and η -Cu₆Sn₅ mixture, and adding Cu increased the number of η -Cu₆Sn₅ grains [15]. MCDONALD et al [16] reported that cooling Sn–4.0Cu solder was associated with two

reactions. The first involved the nucleation and growth of primary η -Cu₆Sn₅, and the second was related to the solidification of the remaining liquid as a eutectic mixture of η -Cu₆Sn₅ and β -Sn. Various reactions leading to formation of η -Cu₆Sn₅ and β -Sn phases have already been reported, but we could not find any reports on the formation of the ε -Cu₃Sn phase in Sn– x Cu solders, where x was 3–4 wt.%.

The formation mechanism of η -Cu₆Sn₅ and ε -Cu₃Sn phases in the Sn–Cu solders during solidification has not been fully understood, especially for the intermetallic phase formation and for the mismatched crystalline orientation relationships. Moreover, little research about the effects of adding Cu on the crystal orientation has been found. Similarly, intermetallic formation effects of orientation on the mechanical properties of Sn-based solders have been little studied with inconclusive results [12–16]. Here, we studied the influence of different Cu contents on the microstructure and the crystallographic orientation of the Sn– x Cu solders ($x=0$ –4.0 wt.%). The pole figures (PF), misorientation angles (MOS), grain orientation spread (GOS) and kernel average misorientation (KAM), and the resulting mechanical properties were measured.

2 Experimental

Sn– x Cu lead-free solders were formed, where x was 0 (pure Sn), 1.0, 3.0 and 4.0 wt.%. The chemical composition and impurities of solder alloys are illustrated in Table 1. The liquidus and solidus temperatures of pure Sn and Sn– x Cu solders, manufactured by KoKi Products Co., Ltd., are shown in Table 2. Samples were melted in an electric arc furnace. The solder bar with a mass of 300 g was melted in a stainless steel crucible at 370 °C. The molten solder was then poured into a permanent mold and naturally cooled down to room temperature. The temperature profile of sample castings is shown in Fig. 1. The melting and solidification temperatures of solder were measured using the DX1000N Yokogawa data logger, with a type K thermocouple.

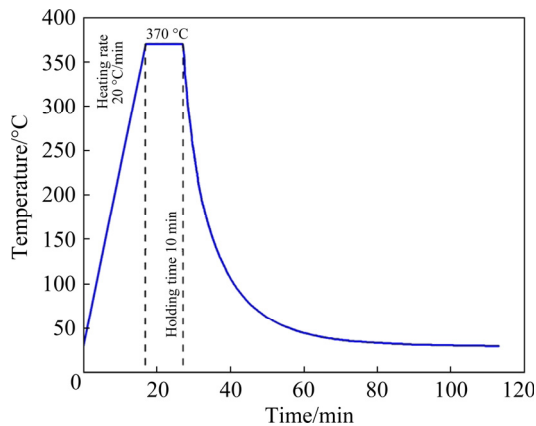
Before examining the microstructure, the specimens were taken in the middle of the mold. The specimens were polished, using a series of SiC grit papers, 800[#], 1000[#] and 1500[#], followed by Al₂O₃ with size of 0.3 μ m. Finally, the polished

Table 1 Chemical composition and impurity of solder alloys

Solder alloy	Main composition/wt. %		Impurity/wt. %												
	Sn	Cu	Pb	Cd	Ni	Sb	Ag	Bi	In	Au	As	Fe	Al	Zn	Ge
Sn–1.0Cu	Bal.	0.70±0.200	≤0.050	≤0.002	0.050±0.030	≤0.100	≤0.100	≤0.100	≤0.100	≤0.050	≤0.030	≤0.001	≤0.001	≤0.001	≤0.001
Sn–3.0Cu	Bal.	3.0±0.500	≤0.050	≤0.002	≤0.010	≤0.100	≤0.010	≤0.100	≤0.100	≤0.050	≤0.030	≤0.020	≤0.001	≤0.001	–
Sn–4.0Cu	Bal.	3.500–4.500	≤0.050	≤0.002	–	≤0.100	≤0.010	≤0.100	≤0.100	≤0.050	≤0.030	≤0.020	≤0.001	≤0.001	–

Table 2 Liquidus and solidus temperatures of pure Sn and Sn–xCu solders

Solder	Solidus temperature/°C	Liquidus temperature/°C
Pure Sn	232	232
Sn–1.0Cu	230	240
Sn–3.0Cu	227	309
Sn–4.0Cu	227	350

**Fig. 1** Temperature profile of sample castings

specimens were ion milled using a Hitachi IM4000 Plus Ar ion milling system. An Olympus BX60M optical microscope was used to examine the microstructure at high magnitudes and a Jeol JSM–5800LV scanning electron microscope (SEM) was used to verify the microstructure. The chemical composition of the microstructure was determined using the Oxford Instruments X-Max energy dispersive spectroscope (EDS). In addition, the lattice structure of the phases was analyzed using the Bruker D8-Discover X-ray diffractometer (XRD).

The crystal and grain orientations were determined by the electron backscatter diffraction (EBSD) using a Hitachi SU8230 field emission scanning electron microscope (FE-SEM) equipped with an Oxford EBSD detector.

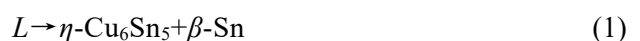
To inspect the mechanical properties, a Zwick, Z020 universal testing machine was used to measure the tensile strength and elongation of the specimens at room temperature, following the ASTM E8M standard. Hardness was measured using a Wilson Tukon 1102 Vickers indenter with a load of 0.2 N and a loading time of 15 s.

3 Results and discussion

3.1 Microstructure and phase formation

FE-SEM images of the solders are shown in Fig. 2. It can be seen that β -Sn and intermetallic phases formed in the solder matrix. In Fig. 2(a), the microstructure of the pure Sn had only a large β -Sn phase. Addition of 1.0 wt.% Cu to the pure Sn led to the β -Sn phase and a smaller intermetallic phase/ β -Sn eutectic area, as shown in Fig. 2(b). The β -Sn phase was nevertheless still dendritic. The coarse dendrites implied that the mixture was cooled well below the solidification point, i.e., reduced undercooling, but the very fine dendrites in the solder matrix were consistent with rapid growth to well below the solidification point, e.g. high undercooling [17]. In addition, the intermetallic phases consisted of η -Cu₆Sn₅ and ε -Cu₃Sn precipitation surrounding the β -Sn dendrites. The small ε -Cu₃Sn phase was encapsulated by the η -Cu₆Sn₅ phase, and smaller fiber-like structures of η -Cu₆Sn₅ and ε -Cu₃Sn were formed in the eutectic area. Due to the fast cooling rate, short solidification time and low Cu content, Cu diffusion in Sn was minimal, resulting in a smaller intermetallic phases.

In the binary Sn–Cu system, three intermetallic phases (η -Cu₆Sn₅, η' -Cu₆Sn₅ and ε -Cu₃Sn) formed and grew in β -Sn matrix. Phase equilibrium at the Sn-rich phase corner is more important eutectic reaction as [18].



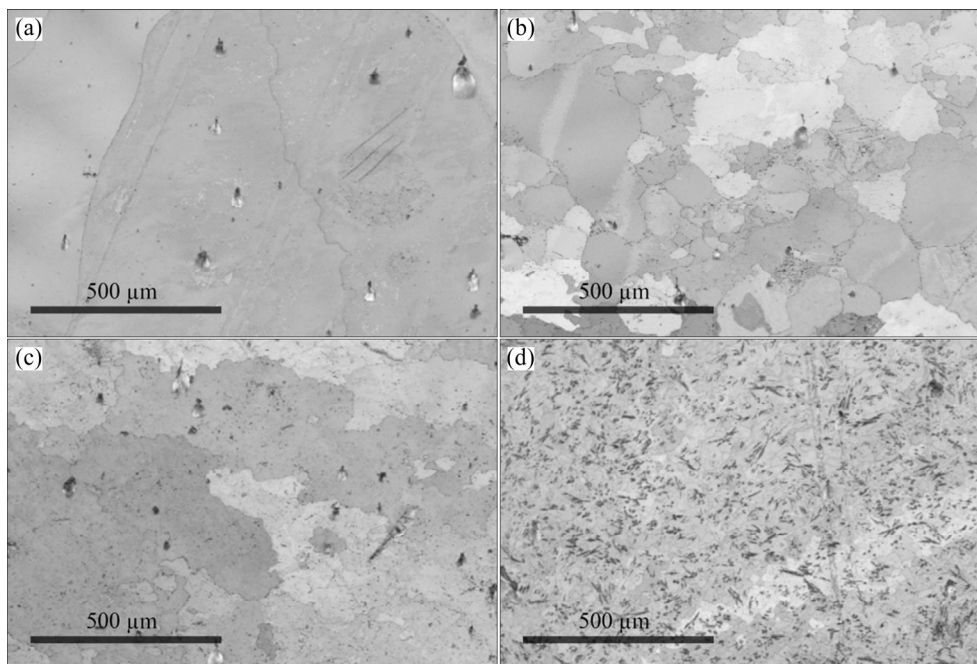
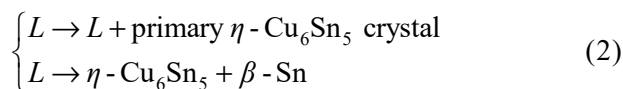


Fig. 2 FE-SEM images of samples: (a) Pure Sn; (b) Sn–1.0Cu; (c) Sn–3.0Cu; (d) Sn–4.0Cu

Previous works [12,14] showed that the dendrites of β -Sn and η -Cu₆Sn₅ only were formed in Sn–0.7Cu and Sn–1.0Cu solders. This was due to an equilibrium solidification process. Moreover, the equilibrium solidification paths are represented by Eq. (1). In this work, no η' -Cu₆Sn₅ was found in the cast specimens, because the η -Cu₆Sn₅ did not have enough time to transform to η' -Cu₆Sn₅ [19].

Therefore, the non-equilibrium solidification of the Sn–1.0Cu hypereutectic alloy exhibited a large number of η -Cu₆Sn₅ lamellar structures, according to Eq. (2). Strong kinetic undercooling, arising from the rapid solidification condition, led to the eutectic point shifting in the direction of the high Cu content. Hence, all alloys experienced a metastable pseudoeutectic solidification as [14]



where L is the liquid phase.

Thus, it was more feasible for η -Cu₆Sn₅ precipitates to occur first, followed by the precipitation of ε -Cu₃Sn, after a period of incubation. At the higher temperature, Sn diffused by a vacancy-diffusion mechanism to combine with Cu and form the ε -Cu₃Sn phase [20]. Thus, it was also possible, that ε -Cu₃Sn appeared based on the peritectic reaction formulated as



where S_1 is the solid phase of ε -Cu₃Sn, and S_2 is the solid phase of η -Cu₆Sn₅.

The liquid (L) plus solid phase of ε -Cu₃Sn (S_1) transforms into η -Cu₆Sn₅ (S_2) under non-equilibrium cooling conditions. The reason that the peritectic reaction more easily occurs in regions, closer to the cooled surface of the casting, once such regions are Cu-enriched, is due to the inverse segregation [21]. Additionally, in the Sn–Cu system, the peritectic product is an intermetallic phase or has a very narrow homogeneity range [22]. Thus, the microstructure of the solder contained very small amounts of ε -Cu₃Sn phase, encapsulated by the peritectic reaction, and our results were similar to those reported by MEHREEN et al [23], where the ε -Cu₃Sn phase was encapsulated by the peritectic η -Cu₆Sn₅ phase, which was, in turn, surrounded by a eutectic mixture of β -Sn and η -Cu₆Sn₅.

In Fig. 2(c), large rod- and fiber-like structures of intermetallic phases formed when adding 3.0 wt.% Cu to form Sn–3.0Cu. However, as the Cu content increased with the volume fraction of the η -Cu₆Sn₅ phase, subsequent intermetallic growth noticeably destroyed the dendritic structures. Similarly, adding 4.0 wt.% Cu led to no detectable β -Sn dendrites, due to the higher Cu content, which promoted the intermetallic phase formation and prevented growth of β -Sn dendrites.

The microstructures of 4.0 wt.% Cu are shown in Fig. 2(d). It can be seen that both the η -Cu₆Sn₅ and ε -Cu₃Sn became larger and the volume fraction increased. The solidification time of Sn–4.0Cu was longer than that of Sn, Sn–1.0Cu, and Sn–3.0Cu solders, leading to higher atomic diffusion. Thus, intermetallic phase formation and growth happened more easily with an increase of Cu element and longer solid cooling time. The elemental compositions of the pure Sn, β -Sn, η -Cu₆Sn₅, and ε -Cu₃Sn were determined by EDS. The Cu contents of the η -Cu₆Sn₅ phase ranged from 50.86 to 52.88 at.%, in the ε -Cu₃Sn region, the Cu content was from 73.07 to 76.11 at.% Cu with the remainder being Sn. The XRD diffraction pattern of Sn–4.0Cu is displayed in Fig. 3. The lattice structure and parameters and intermetallic phases from XRD are shown in Table 3. In addition, the β -Sn phase had a body centered tetragonal structure and the Cu phase was α -Cu, with a face-centered cubic structure. Both η -Cu₆Sn₅ and ε -Cu₃Sn phases had a hexagonal structure.

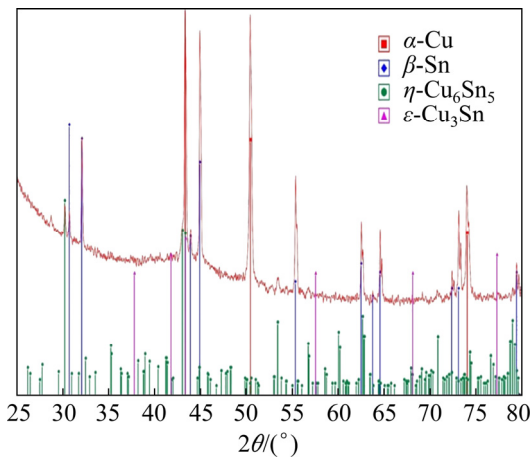


Fig. 3 XRD pattern of Sn–4.0Cu solder

Table 3 XRD analysis of β -Sn, α -Cu and intermetallic phases

Phase	Structure	Pearson symbol	Space group	Lattice parameter/nm
β -Sn	BCT	tI4	141amd (141)	$a=b=0.58340$, $c=0.31505$
α -Cu	FCC	cF4	$Fm\bar{3}m$ (225)	$a=b=c=0.36505$
η -Cu ₆ Sn ₅	NiAs hexagonal	hP4	$P63/mmc$ (194)	$a=0.42000$, $c=0.50900$
ε -Cu ₃ Sn	Hexagonal	–	Gamma	$a=b=0.27490$, $c=0.43220$

3.2 Crystallographic orientation and texture

Figure 4 shows the phases and grain boundaries of the samples, obtained from EBSD phase mapping, where the red region represents β -Sn, and yellow and blue regions represent η -Cu₆Sn₅ and ε -Cu₃Sn phases, i.e. the fraction of β -Sn phase for the pure Sn was 99.80% and the remainder was not detected by EBSD, within the white region, due to defects during specimen preparation. The fractions of phases of all samples are shown in Table 4. In fact, the phase fraction of intermetallic phases (η -Cu₆Sn₅ and ε -Cu₃Sn) and β -Sn phases of the samples increased with Cu content. Therefore, introducing a small Cu content (1.0 and 3.0 wt.%) into the pure Sn, resulted in a small phase fraction of ε -Cu₃Sn phase.

Figure 4 illustrates the grain boundary maps of specimens with different Cu contents. The low-angle boundaries (LAGBs), with misorientation angles $<15^\circ$, are shown as black lines and the high angle boundaries (HAGBs) with disorientation angles $>15^\circ$. In this study, the HAGBs are divided into two groups: misorientation angles of 15° – 50° shown as blue lines and misorientation angles greater than 50° shown as purple lines. A majority of the boundaries were identified as HAGB, for the pure Sn, Sn–1.0Cu and Sn–3.0Cu. In contrast, the Sn–4.0Cu solder had more LAGB, due to numerous fine η -Cu₆Sn₅ phases, embedded into the individual β -Sn, which distorted the lattice more severely in the as-cast microstructure [24].

The preferred orientation of the β -Sn, η -Cu₆Sn₅ and ε -Cu₃Sn phases is shown in Figs. 5, 6 and 7. The crystallographic texture (i.e. grain orientation) of the different Cu contents, in terms of multiples of uniform distribution (MUD), was derived from the pole figure. A larger degree of preferred orientation was shown by the higher MUD (red) regions. The pole figure of the β -Sn phase, of all solders in Fig. 5, showed that strong $\{001\}$ plane of the β -Sn phase was the preferred orientation. The texture strength of β -Sn on the $\{001\}$ plane was consistent with that reported by XIAN et al [25] and BIELER and TELANG [26]. To prove the β -Sn phase having the preferred orientation in $\{001\}$ plane, the inverse pole figures are shown in Fig. 8. Moreover, the planes were mismatched, due to the thermal expansion, strain and the deformation leading to a change in preferred orientation of the plane family [26,27]. Our results revealed that added Cu

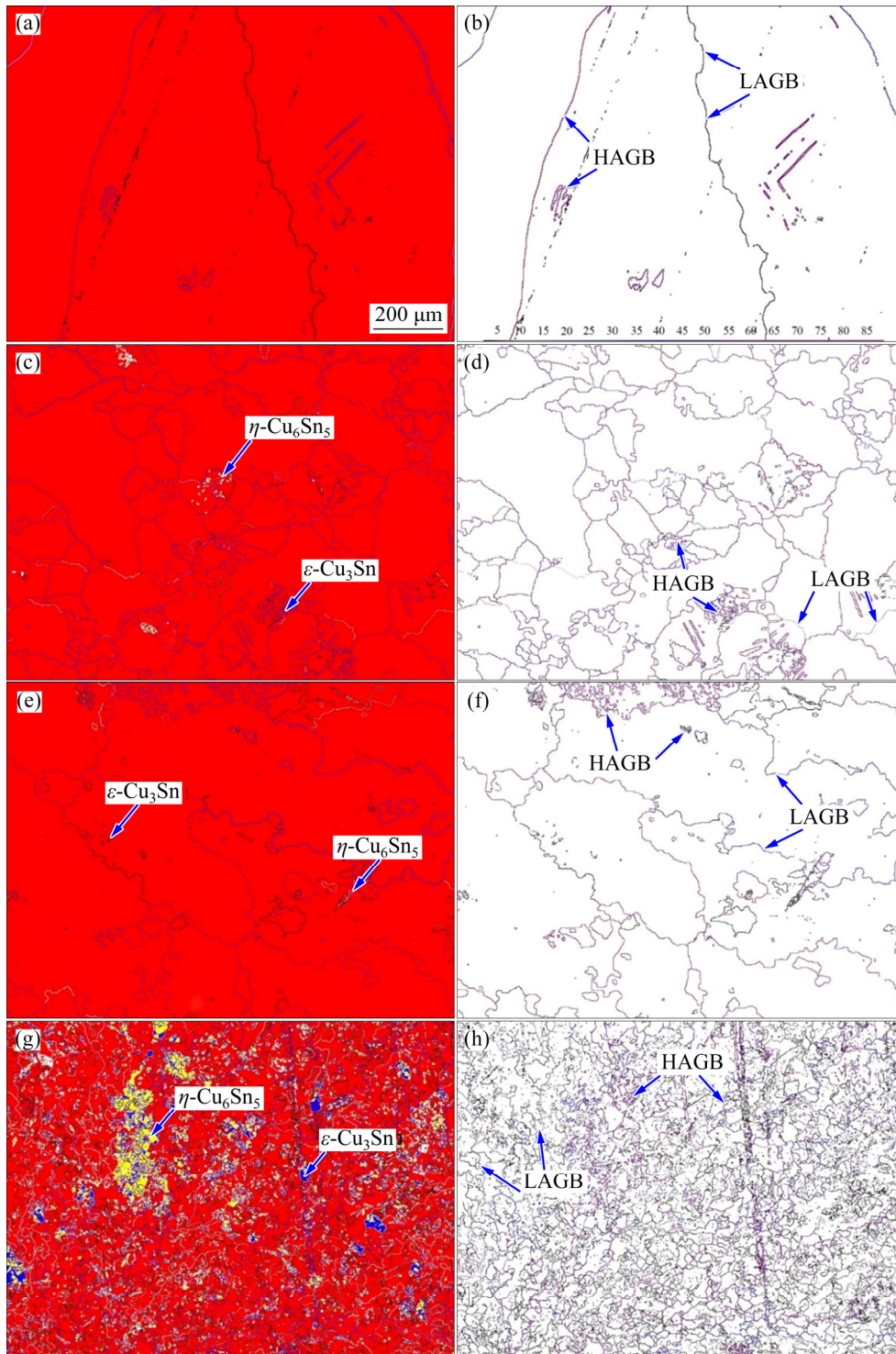


Fig. 4 Phases and grain boundaries of samples: (a, b) Pure Sn; (c, d) Sn–1.0Cu; (e, f) Sn–3.0Cu; (g, h) Sn–4.0Cu

Table 4 Phase fraction of all samples (%)

Solder	β -Sn	ϵ -Cu ₃ Sn	η -Cu ₆ Sn ₅	Defect of preparation
Pure Sn	99.80	–	–	Balance
Sn–1.0Cu	99.20	0.00101	0.08970	Balance
Sn–3.0Cu	99.10	0.00279	0.01390	Balance
Sn–4.0Cu	87.60	4.06000	5.59000	Balance

did not change the dominant plane of the β -Sn phase.

In Fig. 6, after adding 1.0 wt.% Cu, the η -Cu₆Sn₅ could be formed into the {0001} or {10 $\bar{1}$ 0} planes, but it easily grew into the {0001} plane, because it contained η -Cu₆Sn₅, surrounded by β -Sn. The intermetallic phase of η -Cu₆Sn₅, appeared

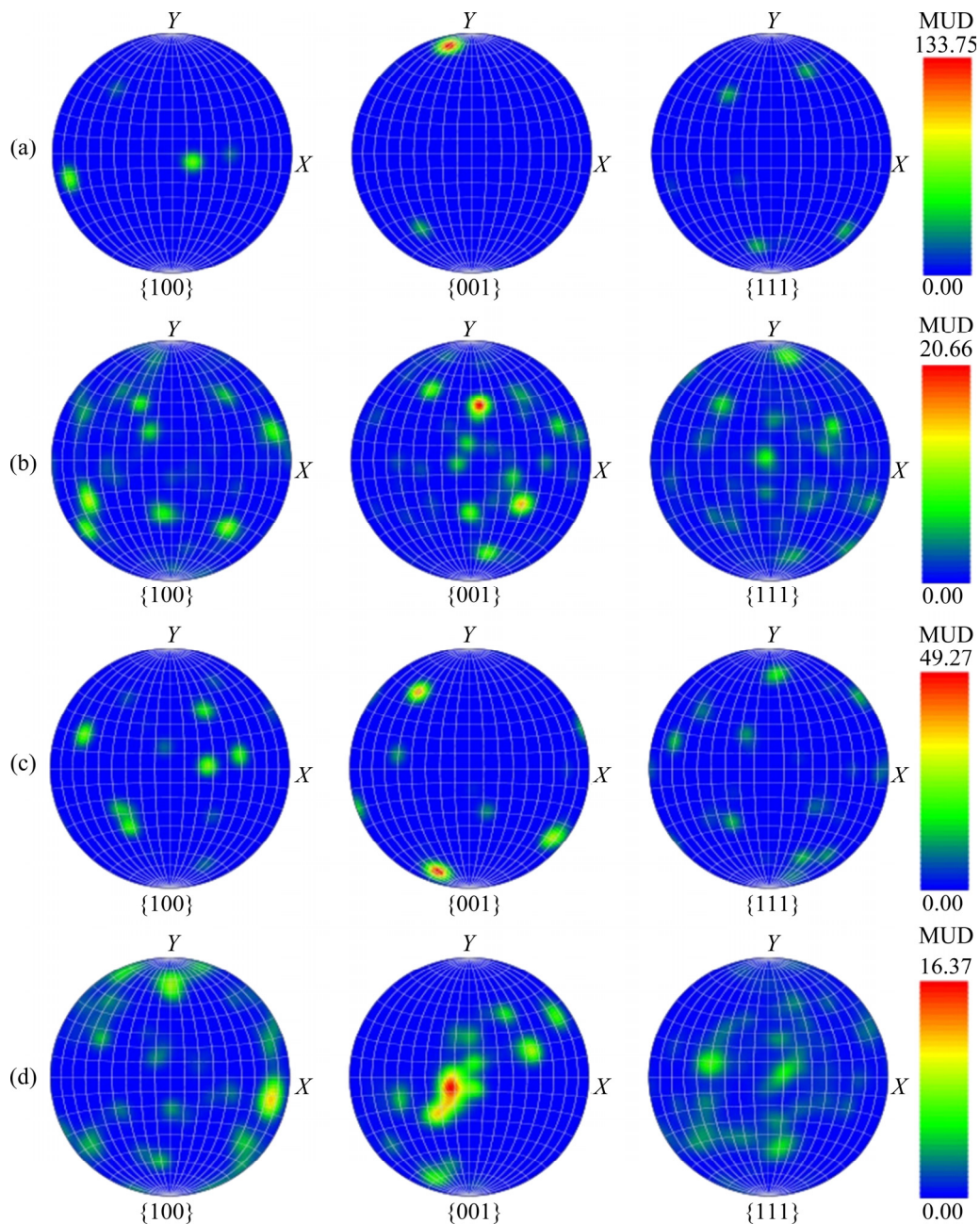


Fig. 5 Pole figures of β -Sn phase: (a) Pure Sn; (b) Sn-1.0Cu; (c) Sn-3.0Cu; (d) Sn-4.0Cu

as a fibrous and more random texture, which was consistent with the reports by XIAN et al [25]. Due to the η -Cu₆Sn₅ growth, the $\{10\bar{1}0\}$ plane was sometimes found after cooling [28], due to the short solidification time and a low Cu content in the molten solder [28,29].

For the 3.0 and 4.0 wt.% Cu, the η -Cu₆Sn₅ exhibited the preferred $\{0001\}$ orientation transfer to the $\{010\}$ plane. The transformation of orientation, due to the η -Cu₆Sn₅ grain growth and the η -Cu₆Sn₅ ‘scallop’ can be tilted easily, because they are surrounded by liquid solder [30]. Thus, the intermetallic growth led to residual strain and

change of preferred orientation plane. The preferred orientation in our work was also observed by LIU and JI [24] in Sn-0.5Cu solder. In addition, the ε -Cu₃Sn for all solders had a preferred orientation of $\{0001\}$ plane as shown in Fig. 7. Furthermore, the orientation distribution of intermetallic phases (η -Cu₆Sn₅ and ε -Cu₃Sn) became less uniform with increased Cu content: the higher Cu content improved intermetallic phase formation and affected the green regions of the pole figures, where spread of the less uniform distribution was found for all planes, leading to the subsequent reduced MUD value, which equated to a lower degree of

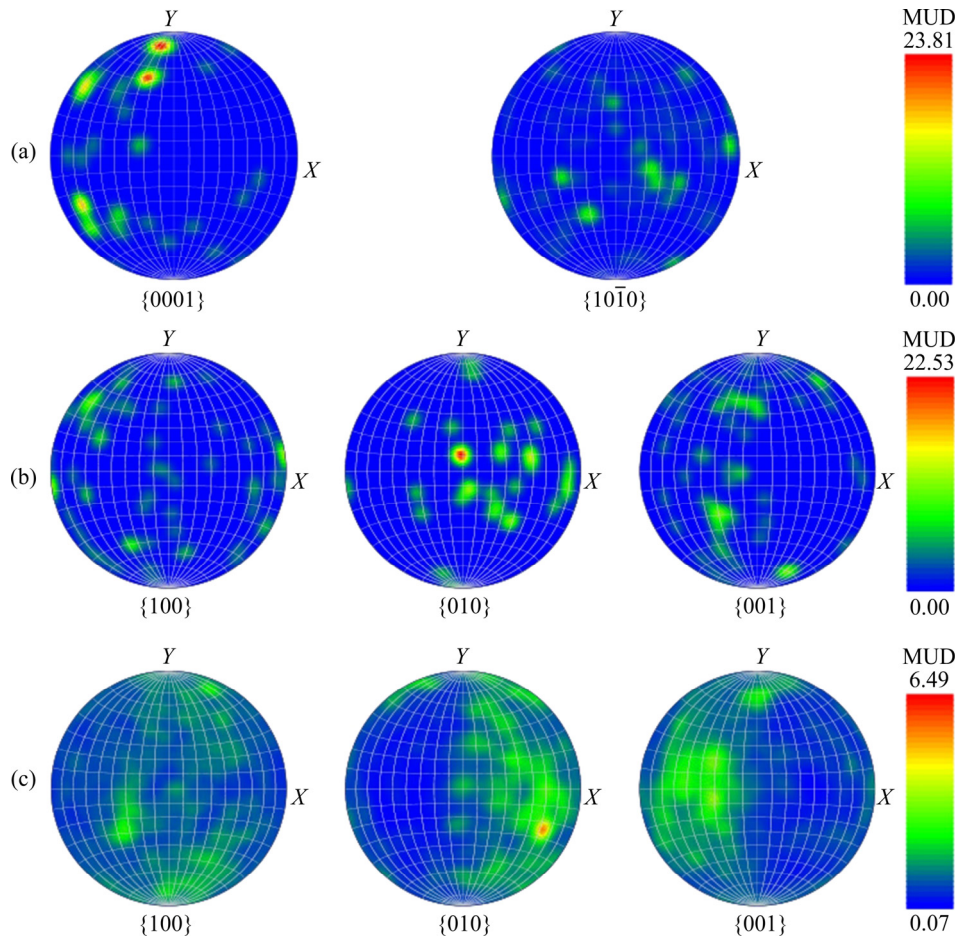


Fig. 6 Pole figures of η -Cu₆Sn₅ phase: (a) Sn–1.0Cu; (b) Sn–3.0Cu; (c) Sn–4.0Cu

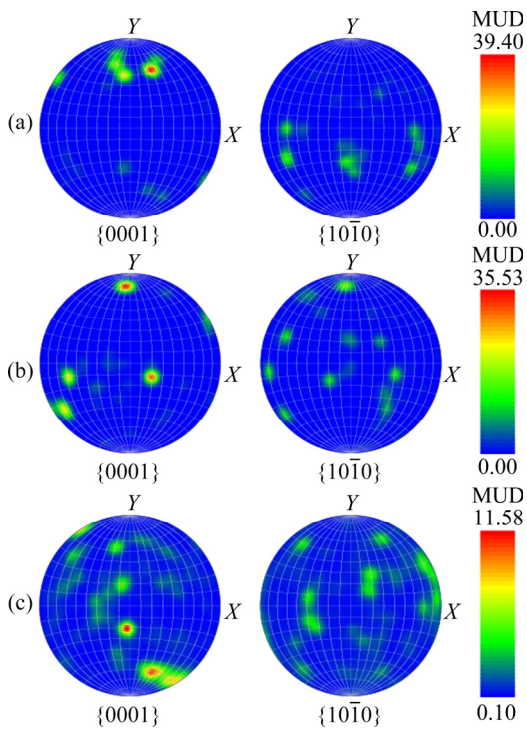


Fig. 7 Pole figures of ε -Cu₃Sn phase: (a) Sn–1.0Cu; (b) Sn–3.0Cu; (c) Sn–4.0Cu

preferred orientation or texture of microstructures.

The formation of an intermetallic phase in a solder matrix and the orientation relationship between β -Sn and the intermetallic phase formed during the solder cooling stage [31]. The orientation of the intermetallic phases also appears to be random over different β -Sn grain orientations. The nucleation orientation relationship and growth texture of β -Sn, η -Cu₆Sn₅ and ε -Cu₃Sn are consistent with the preferred growth planes.

Sn–1.0Cu solder:

$$\begin{aligned} & \{0001\}_{\eta\text{-Cu}_6\text{Sn}_5} // \{001\}_{\beta\text{-Sn}}, \\ & \{0001\}_{\eta\text{-Cu}_6\text{Sn}_5} // \{0001\}_{\varepsilon\text{-Cu}_3\text{Sn}} \end{aligned} \quad (4)$$

Sn–3.0Cu solder:

$$\begin{aligned} & \{010\}_{\eta\text{-Cu}_6\text{Sn}_5} // \{001\}_{\beta\text{-Sn}}, \\ & \{010\}_{\eta\text{-Cu}_6\text{Sn}_5} // \{0001\}_{\varepsilon\text{-Cu}_3\text{Sn}} \end{aligned} \quad (5)$$

Sn–4.0Cu solder:

$$\begin{aligned} & \{010\}_{\eta\text{-Cu}_6\text{Sn}_5} // \{001\}_{\varepsilon\text{-Cu}_3\text{Sn}}, \\ & \{010\}_{\eta\text{-Cu}_6\text{Sn}_5} // \{0001\}_{\varepsilon\text{-Cu}_3\text{Sn}} \end{aligned} \quad (6)$$

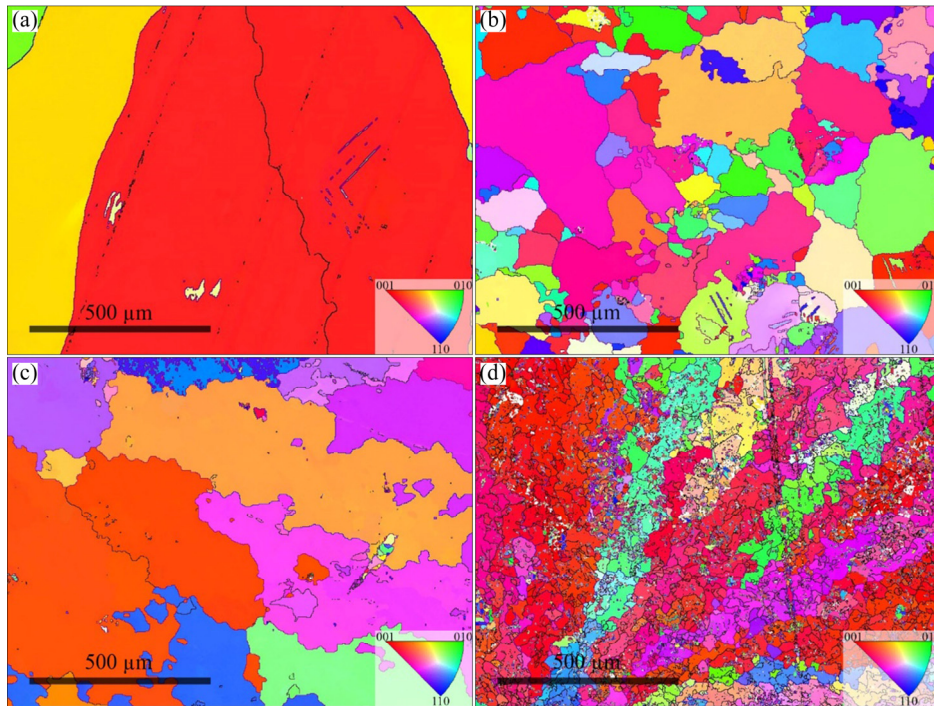


Fig. 8 Inverse pole figures of β -Sn phase: (a) Pure Sn; (b) Sn–1.0Cu; (c) Sn–3.0Cu; (d) Sn–4.0Cu

However, two types of η -Cu₆Sn₅ crystals in 3.0 and 4.0 wt.% Cu had almost hexagonal rods and fibers in the morphology, with $\{0001\}$ Cu₆Sn₅ showing long fibers, nearly parallel to the sample surface, and η -Cu₆Sn₅ ‘rods’ perpendicular to the main $\{001\}$ Sn plane. The orientation relations between η -Cu₆Sn₅ face morphology and β -Sn are

$$\{1\bar{1}00\}_{\eta\text{-Cu}_6\text{Sn}_5} // \{001\}_{\beta\text{-Sn}} \quad (7)$$

$$\{0001\}_{\eta\text{-Cu}_6\text{Sn}_5} \perp \{001\}_{\beta\text{-Sn}} \quad (8)$$

Moreover, the β -Sn grains were larger than the intermetallic grains, indicating that the intermetallic phase grew on the β -Sn grains. The grains of the intermetallic Sn–*x*Cu alloy phases are seen in Fig. 4. In addition, the orientation of the intermetallic phase was random over different β -Sn grain orientations, as illustrated in Fig. 9, i.e., there was no preferred orientation between η -Cu₆Sn₅ faces and the β -Sn matrix. SIDHU et al [32] also observed that the Ag₃Sn phase was randomly dispersed in the β -Sn matrix and showed no preferred orientation to the Ag₃Sn phase and the β -Sn matrix. However, η -Cu₆Sn₅ grains were larger (average diameter 9.073 μm) than the ε -Cu₃Sn grains (8.979 μm), which was consistent with the results reported by SHANG et al [31], and ε -Cu₃Sn grains can grow by consuming neighboring η -Cu₆Sn₅: the crystal structures also differed. Clearly, the coarsening of

ε -Cu₃Sn grains on the η -Cu₆Sn₅ phase was influenced by the orientation-preferred surrounding neighbors and caused the different crystal structures. A preference for similar crystal structures, with minimal lattice mismatch, drove the ε -Cu₃Sn phase to grow by consuming the neighboring η -Cu₆Sn₅ phase [31]. The strong orientation relationship between η -Cu₆Sn₅ and ε -Cu₃Sn suggested that, at the nucleation stage, η -Cu₆Sn₅ formed prior to the ε -Cu₃Sn [30].

The growth rate of η -Cu₆Sn₅ crystal faces in the longitudinal direction was larger than that in the transversal direction, due to the surface density of the plane, i.e., the surface density of the $\{10\bar{1}0\}$ plane (9.472 nm^{-2}) is higher than that of the $\{0001\}$ plane (6.571 nm^{-2}): crystals tend to grow parallel to the net plane, with the largest surface density [33]. On the other hand, the anisotropic growth of intermetallic crystals tended to grow anisotropically in the longitudinal direction, i.e., η -Cu₆Sn₅ crystals grew along the $[0001]$ axis. Additionally, grains with greater angle differences caused large lateral dimensions [34]. Therefore, with the higher Cu content, poorly oriented grains tended to be larger, causing growth of the intermetallic phases.

The β -Sn grain orientations were randomly distributed as shown in Fig. 10. For the pure Sn,

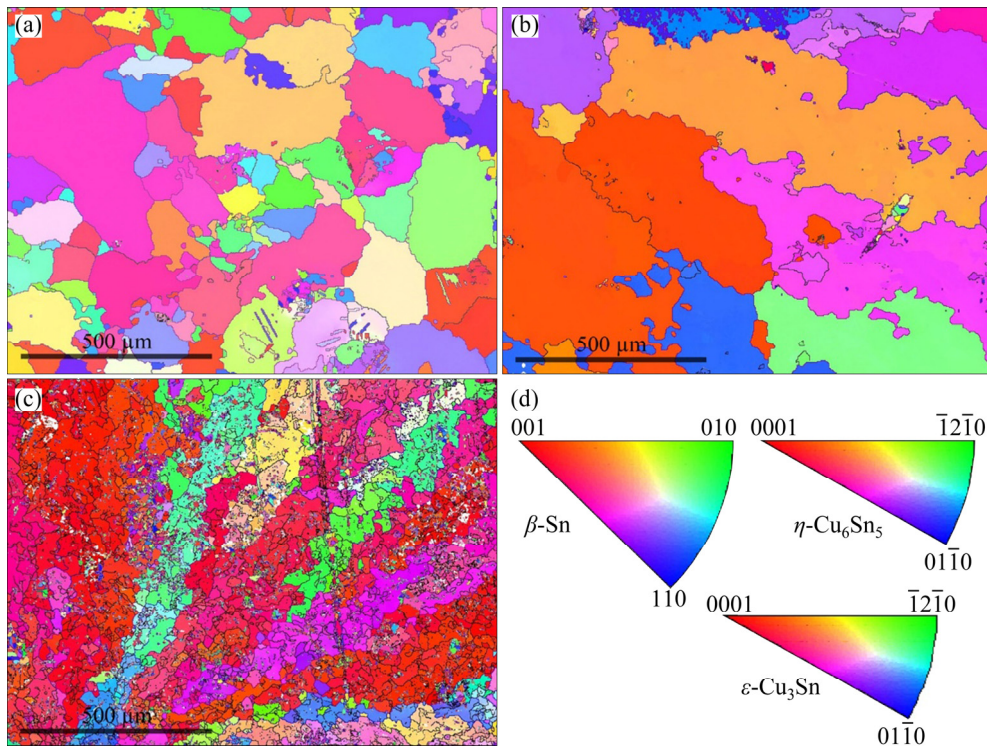


Fig. 9 Microstructure orientation maps: (a) Sn–1.0Cu; (b) Sn–3.0Cu; (c) Sn–4.0Cu; (d) Inverse pole figures

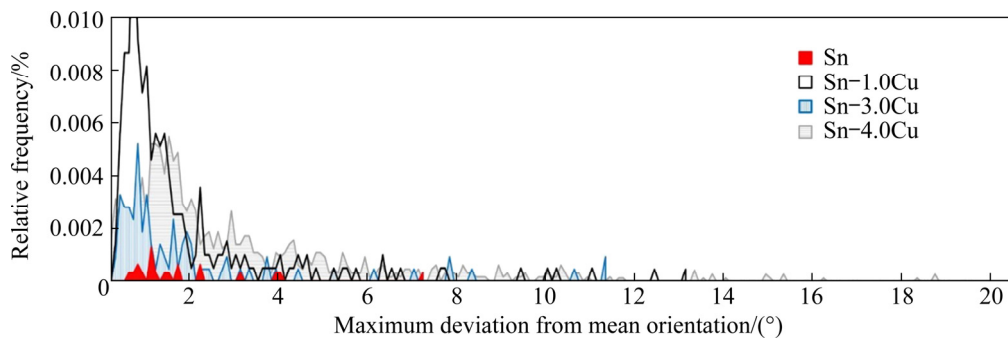


Fig. 10 Mean orientation spread and distribution orientation deviations for β -Sn

the poor orientations of grain boundaries were mostly found in the range of 0° – 7.05° , whereas, in 1.0–3.0 wt.% Cu, a slightly increased density of LAGBs and poor orientations were found in the range of 0° – 14° . However, adding 4.0 wt.% Cu to Sn led to a higher density of LAGBs in our study. In addition, the poorly oriented grain boundaries were found mostly in the range of 0° – 20.5° . However, all samples showed a misorientation peak at 0.5° – 1.5° . The density of small grains, with LAGB microstructures, increased as the Cu content increased. With the higher Cu content, under solidification, there was a significant influence on the configuration of β -Sn grains. Most β -Sn grains had LAGBs structures, with high dislocation densities and strains [35,36].

However, adding 1.0–3.0 wt.% Cu to Sn led to no misorientations of η -Cu₆Sn₅ and ε -Cu₃Sn, because of small intermetallic phase formation. Figure 11 illustrates the misorientation angles of the η -Cu₆Sn₅ and ε -Cu₃Sn phases with higher Cu content. The η -Cu₆Sn₅ phase exhibited few misorientations, and the high misorientations of the ε -Cu₃Sn phase indicated the development of a large ε -Cu₃Sn phase.

The grain orientation spread is shown in false color maps in Fig. 12. Different colors represent different orientation spreads or in-grain misorientations, as the grains deformed or recrystallized. The low orientation spreads represent large grain formation (overgrown grains) and the high orientation spreads represent relatively fine

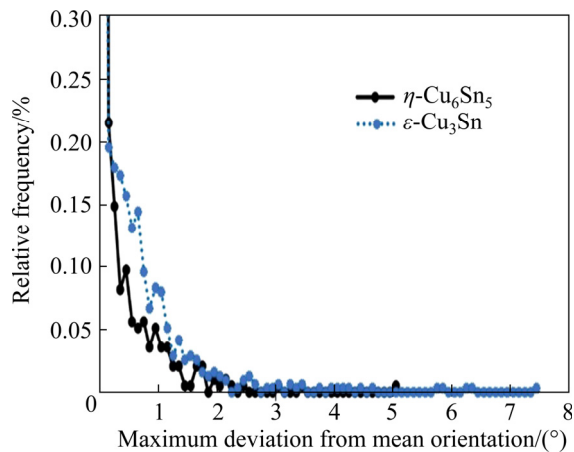


Fig. 11 Mean orientation spread of η - Cu_6Sn_5 and ε - Cu_3Sn phases

grains [37]. LIU and JI [24] reported that spread $<1.5^\circ$ represented recrystallized grains, whereas non-recrystallized grains had spread $>1.5^\circ$. Moreover, the sub-grain formation interior had non-recrystallized grain with LAGBs $\sim 2^\circ$ – 15° [24]. LAGBs developing near grain boundaries helped to form sub-boundaries [38].

For the pure Sn, the main stream of the grain area appeared in red, representing a lower spread. Other grains, with an overall low spread

$<1.0^\circ$, implied that grains recrystallized. This suggested that the addition of Cu to the pure Sn affected the deformed grains of the solder. In the 1.0–3.0 wt.% Cu range, the sub-grains were retarded by small intermetallic particles after deformation, leading to an increase in misorientation angles of the grain boundary and GOS values, due to the dislocations extensively trapped in boundaries [24]. With a higher Cu content, more sub-grain developed due to dense intermetallic particles, which were widely spaced in the Sn grain interiors. This led to an impedance in the growth of the nuclei and subsequently inhibited the occurrence of grain growth. The ε - Cu_3Sn exhibited better GOS values and distribution than the η - Cu_6Sn_5 , as shown in Fig. 13.

Thus, more angled boundaries and GOS values lead to the subsequent increase in sub-grains. This implied that the atoms readily diffused across the fine-grained structure. This further suggested that Cu facilitated the formation of different special boundaries with different boundary energies [39].

The kernel average misorientation (KAM) displays the local strain distribution in each grain. The distribution of the grain boundary vs Cu content is shown in Fig. 14. Green regions show

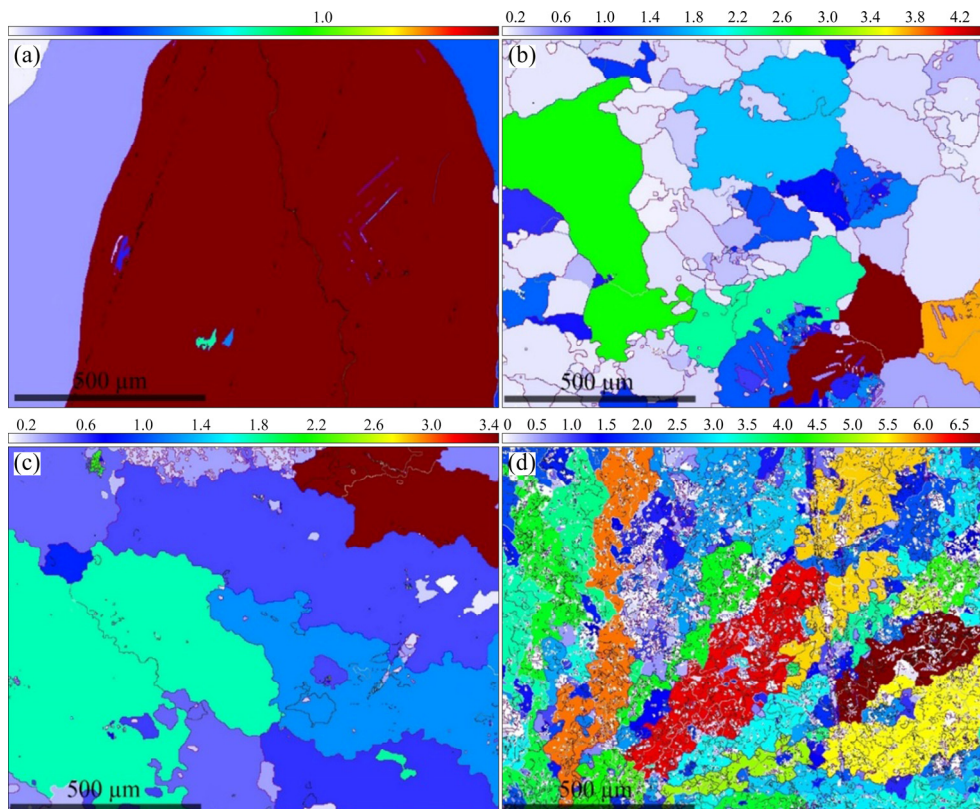


Fig. 12 GOS analysis of β -Sn: (a) Pure Sn; (b) Sn–1.0Cu; (c) Sn–3.0Cu; (d) Sn–4.0Cu

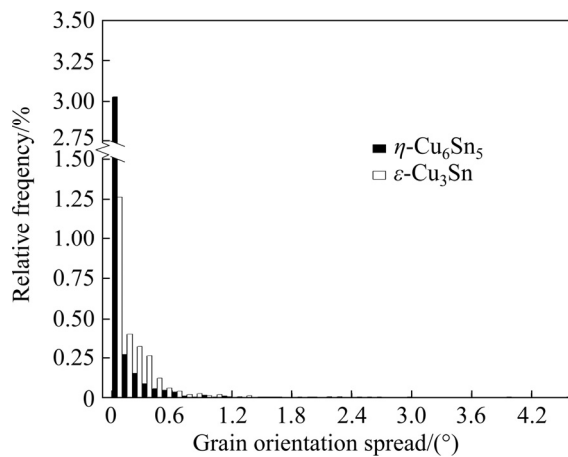


Fig. 13 Grain orientation spread of η - Cu_6Sn_5 and ε - Cu_3Sn phases

higher KAM values. The pure Sn showed residual strain, due to low-energy boundaries with deformed grains [40]. After adding Cu, the stored strain increased with Cu content. The increased number of the low-angle boundaries indicated that the dislocation density increased as the deformation continued [36].

3.3 Mechanical properties and fracture behavior

The relationship between tensile stress and strain is illustrated in Fig. 15. The relationship between tensile strength and elongation for all

samples is shown in Fig. 16. The Sn- x Cu solders exhibited significantly better tensile strengths than the pure Sn. However, the elongation decreased as Cu content increased. This was attributed to the intermetallic phases (η - Cu_6Sn_5 and ε - Cu_3Sn) in the solder matrix acting as the reinforced phase of the solder alloy, but elongation deteriorated because of the inherited brittleness. Figure 17 shows the surface fractures for different Cu contents. The specimens showed ductile fracture with low Cu contents and the brittle fracture with high Cu contents. In particular, the Sn-4.0Cu solder fracture surface shows a flat smooth fracture surface, indicating brittle fracture. The fractured surface and dimples confirmed that dimple size increased with high Cu contents. However, the fracture occurred in the intermetallic phase and then extended into the adjacent solder matrix [41]. Thus, the ductility and brittleness was associated with the various slip systems encountered in crystalline structures. The solder matrix had more β -Sn phase with body centred tetragonal structures compared to the large intermetallic phases with hexagonal close packed structures, which exhibited transition fractures from ductile to brittle, due to the slip system in solder. Sn can access up to ten different slip systems, whereas hexagonal close packed structures show only six slip systems [24,42,43]. More slip systems offer a

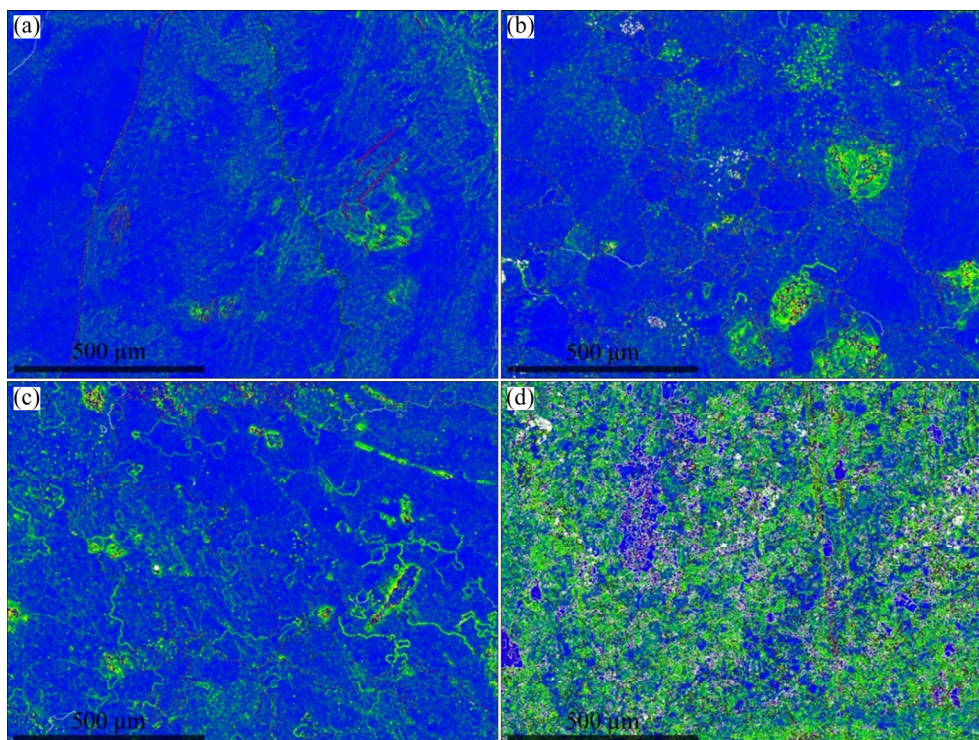


Fig. 14 KAM mapping of samples: (a) Pure Sn; (b) Sn-1.0Cu; (c) Sn-3.0Cu; (d) Sn-4.0Cu

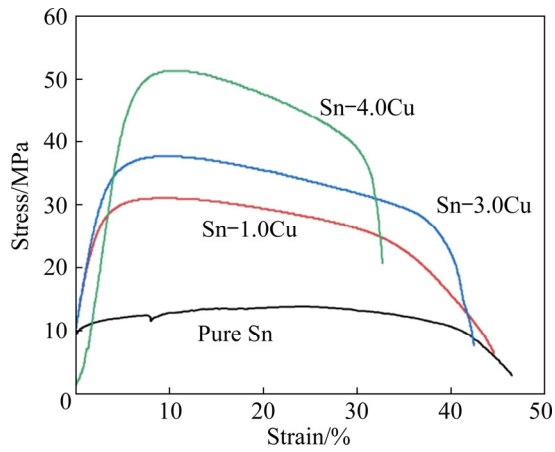


Fig. 15 Stress–strain curves of solders

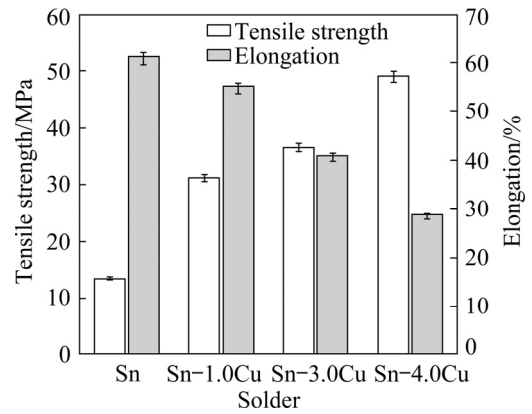


Fig. 16 Effect of Cu addition to pure Sn on tensile strength and elongation

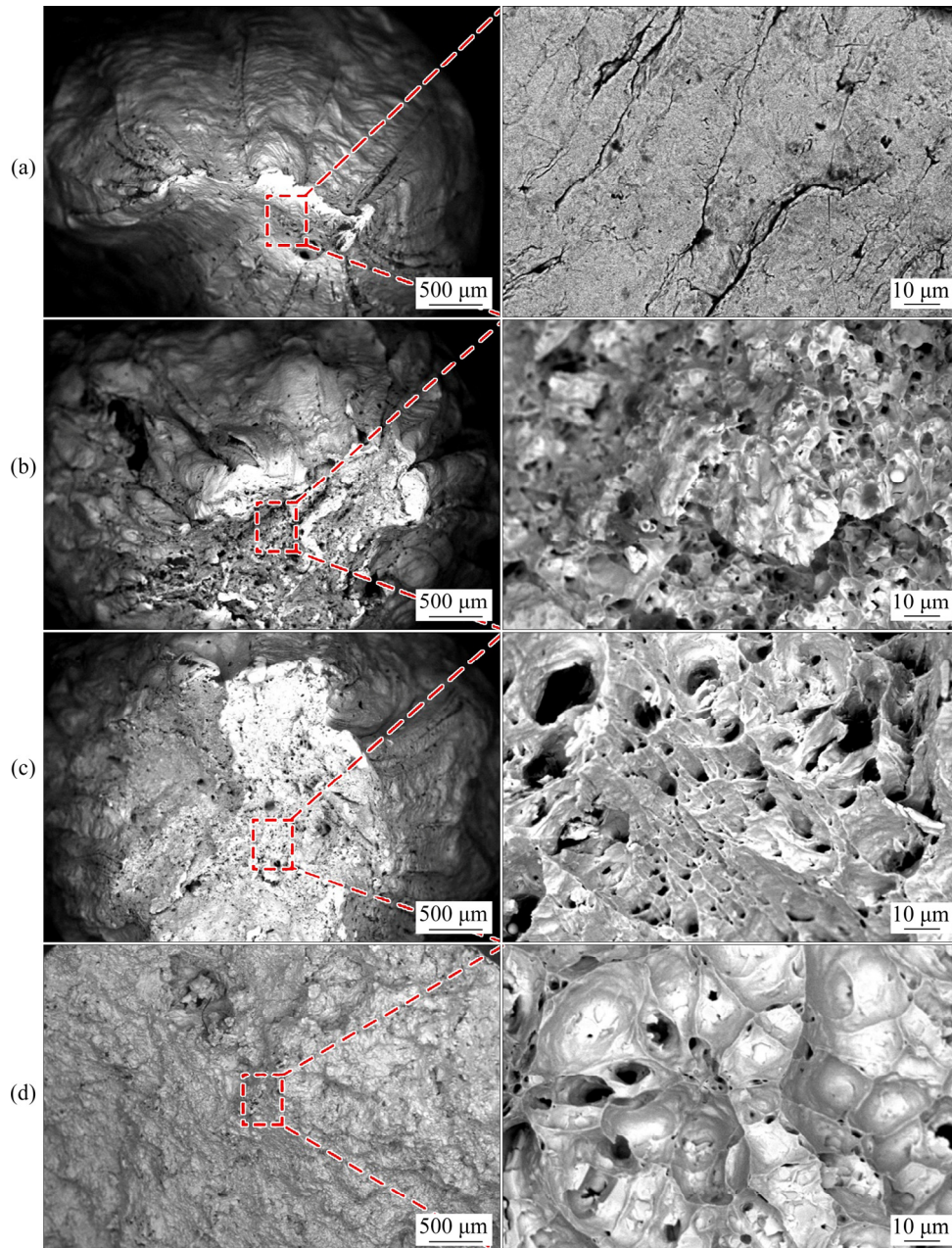


Fig. 17 SEM images of fractured surface: (a) Pure Sn; (b) Sn-1.0Cu; (c) Sn-3.0Cu; (d) Sn-4.0Cu

greater potential for dislocation and ductile fracture. In addition, a large strain fracture occurred at the grain boundary, and ductile fracture was predominantly transgranular, i.e. through the grain. In conjunction, the high Cu content resulted in the high microhardness, as shown in Fig. 18. High microhardness in the intermetallic phases can also increase the tensile strength and microhardness of the solder because the intermetallic phases were intrinsically hard [44]. Reported hardnesses were, 10 KHN for Sn, 389 KHN for η -Cu₆Sn₅, and 573 KHN for ε -Cu₃Sn [45]. Thus, the volume fraction of the β -Sn represented a ductility phase reduction, but the intermetallic phase with a higher hardness area increased, leading to a more brittle structure.

In summary, by adding appropriate amount of Cu to Sn-based solder, the properties of solders, i.e. the microstructure, the orientation, and the mechanical properties of the material can be adjusted.

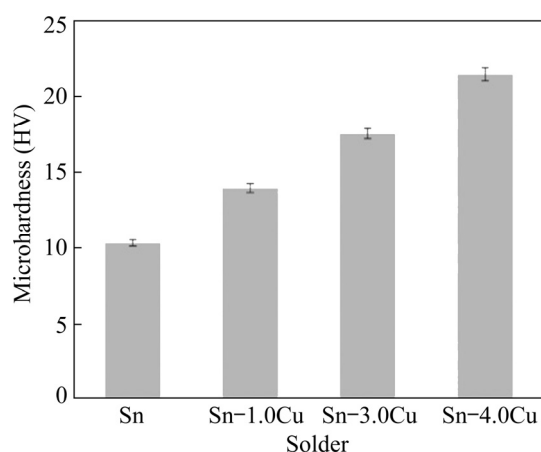


Fig. 18 Effect of Cu addition to pure Sn on microhardness

4 Conclusions

(1) With 1.0 wt.% Cu added, the β -Sn dendritic and intermetallic phases or β -Sn eutectic areas were detected in the solder microstructure, and the intermetallic phases consisted of η -Cu₆Sn₅ and ε -Cu₃Sn precipitation, surrounding the β -Sn dendrites.

(2) No β -Sn dendrites were found, when there were 3.0 and 4.0 wt.% Cu, and η -Cu₆Sn₅ and ε -Cu₃Sn regions became larger in β -Sn matrix area.

(3) The intermetallic phases formed were η -Cu₆Sn₅ and ε -Cu₃Sn. Both the η -Cu₆Sn₅ and ε -Cu₃Sn intermetallic phases, with a hexagonal

crystal structure, were detected in the microstructure of the Sn-*x*Cu solders. The β -Sn phases with body centred tetragonal structures were present.

(4) The phase fraction of β -Sn and grain size decreased with increased Cu content.

(5) The preferred orientation of the β -Sn in all solders was the {001} plane. With the addition of 1.0 wt.% Cu, the η -Cu₆Sn₅ phase showed primarily {0001} plane. At 3.0 or 4.0 wt.% Cu, the η -Cu₆Sn₅ had a preferred {010} orientation. In addition, the ε -Cu₃Sn phase only showed {0001} plane.

(6) High content of Cu in solder supported the growth of total intermetallic phases and low-angle grain boundaries (LAGB), strong preferred orientation, and residual strain, leading to improved tensile strength and microhardness.

Acknowledgments

The authors would like to acknowledge Rajamangala University of Technology Rattanakosin and School of Engineering, King Mongkut's Institute of Technology Ladkrabang for the laboratory support of this research, and sincere appreciation was also expressed to KoKi Products Co., Ltd. for material support.

References

- [1] KOTADIA H R, HOWES P D, MANNAN S H. A review: On the development of low melting temperature Pb-free solders [J]. *Microelectronics Reliability*, 2014, 54(6/7): 1253–1273. doi:10.1016/j.microrel.2014.02.025.
- [2] SATOH R, ARAKAWA K, HARADA M, MATSUI K. Thermal fatigue life of Pb–Sn alloy interconnections [J]. *IEEE Transactions on Components, Hybrids, and Manufacturing Technology*, 1991, 14: 224–232. doi:10.1109/33.76537.
- [3] KANG S K, SARKHEL A K. Lead (Pb)-free solders for electronic packaging [J]. *Journal of Electronic Materials*, 1994, 23: 701–707. doi:10.1007/BF02651362.
- [4] TAO Q B, BENABOU L, LE V N, HWANG H, LUU D B. Viscoplastic characterization and post-rupture microanalysis of a novel lead-free solder with small additions of Bi, Sb and Ni [J]. *Journal of Alloys and Compounds*, 2017, 694: 892–904. doi:10.1016/j.jallcom.2016.10.025.
- [5] PECHT M, SHIBUTANI T, WU L F. A reliability assessment guide for the transition planning to lead-free electronics for companies whose products are RoHS exempted or excluded [J]. *Microelectronics Reliability*, 2016, 62: 113–123. doi:10.1016/j.microrel.2016.03.020.
- [6] OSÓRIO W R, LEIVA D R, PEIXOTO L C, GARCIA L R, GARCIA A. Mechanical properties of Sn–Ag lead-free solder alloys based on the dendritic array and Ag₃Sn

- morphology [J]. *Journal of Alloys and Compounds*, 2013, 562: 194–204. doi:10.1016/j.jallcom.2013.02.050.
- [7] SCHON A F, REYES R V, SPINELLI J E, GARCIA A, SILVA B L. Assessing microstructure and mechanical behavior changes in a Sn–Sb solder alloy induced by cooling rate [J]. *Journal of Alloys and Compounds*, 2019, 809: 151780. doi:10.1016/j.jallcom.2019.151780.
- [8] RAMLI M I I, MOHD SALLEH M A A, YASUDA H, CHAI PRAPA J, NOGITA K. The effect of Bi on the microstructure, electrical, wettability and mechanical properties of Sn–0.7Cu–0.05Ni alloys for high strength soldering [J]. *Materials and Design*, 2020, 186: 108281. doi:10.1016/j.matdes.2019.108281.
- [9] HOU N, BELYAKOV S A, PAY L, SUGIYAMA A, YASUDA H, GOURLAY C M. Competition between stable and metastable eutectic growth in Sn–Ni alloys [J]. *Acta Materialia*, 2018, 149: 119–131. doi:10.1016/j.actamat.2018.02.034.
- [10] REEVE K N, HANDWERKER C A. Beta-tin grain formation in aluminum-modified lead-free solder alloys [J]. *Journal of Electronic Materials*, 2018, 47: 61–76. doi:10.1007/s11664-017-5819-8.
- [11] ZENG G, XUE S B, ZHANG L, GAO L L. Recent advances on Sn–Cu solders with alloying elements: Review [J]. *Journal of Materials Science: Materials in Electronics*, 2011, 22: 565–578. doi:10.1007/s10854-011-0291-3.
- [12] MADENI J, LIU S, SIEWERT T. Casting of lead-free solder bulk specimens with various solidification rates [C]//ASM Conference Proceedings: Joining of Advanced and Specialty Materials, 2001: 33–38.
- [13] VENTURA T, TERZI S, RAPPAZ M, DAHLE A K. Effects of solidification kinetics on microstructure formation in binary Sn–Cu solder alloys [J]. *Acta Materialia*, 2011, 59: 1651–1658. doi:10.1016/j.actamat.2010.11.032.
- [14] SHEN J, LIU Y C, GAO H X. Formation of bulk Cu₆Sn₅ intermetallic compounds in Sn–Cu lead-free solders during solidification [J]. *Journal of Materials Science*, 2007, 42: 5375–5380. doi:10.1007/s10853-006-0892-z.
- [15] XIAN J W, BELYAKOV S A, BRITTON T B, GOURLAY C M. Heterogeneous nucleation of Cu₆Sn₅ in Sn–Cu–Al solders [J]. *Journal of Alloys and Compounds*, 2015, 619: 345–355. doi:10.1016/j.jallcom.2014.08.251.
- [16] MCDONALD S, NOGITA K, READ J, VENTURA T, NISHIMURA T. Influence of composition on the morphology of primary Cu₆Sn₅ in Sn–4Cu alloys [J]. *Journal of Electronic Materials*, 2013, 42: 256–262. doi:10.1007/s11664-012-2222-3.
- [17] ANDERSON I E. Development of Sn–Ag–Cu and Sn–Ag–Cu–X alloys for Pb-free electronic solder applications [J]. *Journal of Materials Science: Materials in Electronics*, 2007, 18: 55–76. doi:10.1007/s10854-006-9011-9.
- [18] CHEN S W, WANG C H, LIN S K, CHIU C N. Phase diagrams of Pb-free solders and their related materials systems [J]. *Journal of Materials Science: Materials in Electronics*, 2007, 38: 19–37. doi:10.1007/978-0-387-48433-4_2.
- [19] ZHANG L, LIU Z Q, YANG F, ZHONG S J. Cu₆Sn₅ whiskers precipitated in Sn_{3.0}Ag_{0.5}Cu/Cu interconnection in concentrator silicon solar cells solder layer [J]. *Materials*, 2017, 10: 327. doi:10.3390/ma10040327.
- [20] ABD EL-REHIM A F, ZAHARAN H Y. Investigation of microstructure and mechanical properties of Sn–xCu solder alloys [J]. *Journal of Alloys and Compounds*, 2017, 695: 3666–3673. doi:10.1016/j.jallcom.2016.11.371.
- [21] SPINELLI J E, GARCIA A. Microstructural development and mechanical properties of hypereutectic Sn–Cu solder alloys [J]. *Materials Science and Engineering A*, 2013, 568: 195–201. doi:10.1016/j.msea.2013.01.049.
- [22] ST JOHN D H, HOGAN L M. A simple prediction of the rate of the peritectic transformation [J]. *Acta Metallurgica*, 1987, 35: 171–174. doi:10.1016/0001-6160(87)90226-4.
- [23] MEHREEN S U, NOGITA K, MCDONALD S, YASUDA H, STJOHN D. Suppression of Cu₃Sn in the Sn–10Cu peritectic alloy by the addition of Ni [J]. *Journal of Alloys and Compounds*, 2018, 766: 1003–1013.
- [24] LIU G Y, JI S X. Microstructure, dynamic restoration and recrystallization texture of Sn–Cu after rolling at room temperature [J]. *Materials Characterization*, 2019, 150: 174–183. doi:10.1016/j.matchar.2019.02.032.
- [25] XIAN J W, MA Z L, BELYAKOV S A, OLLIVIER M, GOURLAY C M. Nucleation of tin on the Cu₆Sn₅ layer in electronic interconnections [J]. *Acta Materialia*, 2017, 123: 404–415. doi:10.1016/j.actamat.2016.10.008.
- [26] BIELER T R, TELANG A U. Analysis of slip behavior in a single shear lap lead-free solder joint during simple shear at 25 °C and 0.1/s [J]. *Journal of Electronic Materials*, 2009, 38: 2694–2701. doi:10.1007/s11664-009-0909-x.
- [27] XIAN J W, ZENG G, BELYAKOV S A, GU Q, NOGITA K, GOURLAY C M. Anisotropic thermal expansion of Ni₃Sn₄, Ag₃Sn, Cu₃Sn, Cu₆Sn₅ and β-Sn [J]. *Intermetallics*, 2017, 91: 50–64. doi:10.1016/j.intermet.2017.08.002.
- [28] MA H R, DONG C, CHEN J, WANG Y P, LI X G, MA H T. Mechanism and control of preferred Cu₆Sn₅ growth on single crystal (001)Cu [J]. *Journal of Materials Science: Materials in Electronics*, 2020, 31: 5966–5974. doi:10.1007/s10854-020-03150-y.
- [29] YANG M, CAO Y, JOO S, CHEN H, MA X, LI M. Cu₆Sn₅ precipitation during Sn-based solder/Cu joint solidification and its effects on the growth of interfacial intermetallic compounds [J]. *Journal of Alloys and Compounds*, 2014, 582: 688–695. doi:10.1016/j.jallcom.2013.08.013.
- [30] SUH J O, TU K N, TAMURA N. Preferred orientation relationship between Cu₆Sn₅ scallop-type grains and Cu substrate in reactions between molten Sn-based solders and Cu [J]. *Journal of Applied Physics*, 2007, 102: 1–7.
- [31] SHANG P J, LIU Z Q, LI D X, SHANG J K. Orientation relationships among Sn/Cu₆Sn₅/Cu₃Sn/(111)Cu in the eutectic SnBi/(111)Cu solder joint [C]//11th International Conference on Electronic Packaging Technology & High Density Packaging. Xi'an: IEEE, 2010: 165–169. doi:10.1109/ICEPT.2010.5582454.
- [32] SIDHU R S, MADGE S V, DENG X, CHAWLA N. On the nature of the interface between Ag₃Sn intermetallics and Sn in Sn–3.5Ag solder alloys [J]. *Journal of Electronic Materials*, 2007, 36: 1615–1620. doi:10.1007/s11664-007-0239-9.
- [33] TIAN Y H, ZHANG R, HANG C T, NIU L N, WANG C Q.

- Relationship between morphologies and orientations of Cu_6Sn_5 grains in $\text{Sn}_{3.0}\text{Ag}_{0.5}\text{Cu}$ solder joints on different Cu pads [J]. *Materials Characterization*, 2014, 88: 58–68. doi:10.1016/j.matchar.2013.12.006.
- [34] YANG M, JI H T, WANG S, KO Y H, LEE C W, WU J X, LI M Y. Effects of Ag content on the interfacial reactions between liquid Sn–Ag–Cu solders and Cu substrates during soldering [J]. *Journal of Alloys and Compounds*, 2016, 679: 18–25. doi:10.1016/j.jallcom.2016.03.177.
- [35] ZHAO N, ZHONG Y, DONG W, HUANG M L, MA H T, WONG C P. Formation of highly preferred orientation of β -Sn grains in solidified Cu/SnAgCu/Cu micro interconnects under temperature gradient effect [J]. *Applied Physics Letters*, 2017, 110: 093504 doi:10.1063/1.4977858.
- [36] CHEN H T, YAN B B, YANG M, MA X, LI M Y. Effect of grain orientation on mechanical properties and thermomechanical response of Sn-based solder interconnects [J]. *Materials Characterization*, 2013 85: 64–72. doi:10.1016/j.matchar.2013.07.004.
- [37] AGNOLI A, BERNACKI M, LOGÉ R, FRANCHET J M, LAIGO J, BOZZOLO N. Understanding and modeling of grain boundary pinning in Inconel 718 [C]//International Symposium on Superalloys, 2012: 73–82. doi:10.7449/2012/superalloys_2012_73_82.
- [38] ZHAO Chao, WANG Zhi, PAN De-qing, LI Dao-xi, LUO Zong-qiang, ZHANG Da-tong, YANG Chao, ZHANG Wei-wen. Effect of Si and Ti on dynamic recrystallization of high-performance Cu–15Ni–8Sn alloy during hot deformation [J]. *Transactions of Nonferrous Metals Society of China*, 2019, 29: 2556–2565. doi:10.1016/S1003-6326(19)65163-0.
- [39] TELANG A A, BIELER T T, CHOI S, SUBRAMANIAN K N. Orientation imaging studies of Sn-based electronic solder joints [J]. *Journal of Materials Research*, 2002, 17: 2294–2306. doi:10.1557/JMR.2002.0337.
- [40] TELANG A U, BIELER T R, LUCAS J P, SUBRAMANIAN K N, LEHMAN L P, XING Y, COTTS E J. Grain-boundary character and grain growth in bulk tin and bulk lead-free solder alloys [J]. *Journal of Electronic Materials*, 2004, 33: 1412–1423. doi:10.1007/s11664-004-0081-2.
- [41] HAN Y D, YANG J H, XU L Y, JING H Y, ZHAO L. Effect of transient current bonding on interfacial reaction in Ag-coated graphene Sn–Ag–Cu composite solder joints [J]. *Transactions of Nonferrous Metals Society of China*, 2021, 31: 2454–2467. doi.org/10.1016/S1003-6326(21)65666-2.
- [42] DARBANDI P, BIELER T R, POURBOGHRAT F, LEE T K. Crystal plasticity finite-element analysis of deformation behavior in multiple-grained lead-free solder joints [J]. *Journal of Electronic Materials*, 2013, 42: 201–214. doi:10.1007/s11664-012-2339-4.
- [43] HEBBACHE M. Shear modulus and hardness of crystals: Density functional calculations [J]. *Solid State Communications*, 2000, 113: 427–432. doi:10.1016/S0038-1098(99)00514-1.
- [44] QI L, ZHAO J, WANG X M, WANG L. The effect of Bi on the IMC growth in Sn–3Ag–0.5Cu solder interface during aging process [C]//Proceedings of 2004 International Conference on the Business of Electronic Product Reliability and Liability, 2004: 42–46. doi:10.1109/bepri.2004.1308147.
- [45] OLSEN D, WRIGHT R, BERG H. Effects of intermetallics on the reliability of tin coated Cu, Ag, and Ni parts [C]//13th International Reliability Physics Symposium. Las Vegas, NV, UAS: IEEE, 1975: 80–86. doi:10.1109/IRPS.1975.362679.

Cu 含量对 Sn–xCu 无铅焊料显微组织、晶粒取向和力学性能的影响

Kannachai KANLAYASIRI¹, Niwat MOOKAM²

1. Department of Industrial Engineering, School of Engineering,

King Mongkut's Institute of Technology Ladkrabang, Bangkok 10520, Thailand;

2. Department of Industrial and Production Engineering, Faculty of Industry and Technology,

Rajamangala University of Technology Rattanakosin Wang Klai Kangwon Campus,

Prachuapkhirikhan 77110, Thailand

摘要: 研究 Cu 含量对 Sn–xCu ($x=0\text{--}4.0\%$, 质量分数) 无铅钎料显微组织、晶粒取向和力学性能的影响。结果表明, Cu 的加入诱导了金属间化合物相的形成。 β -Sn 基体中仅含有 η - Cu_6Sn_5 和 ε - Cu_3Sn 相。对于所有 Cu 含量的样品, β -Sn 相沿 {001} 面形成强的择优取向。当 Sn 中掺杂 1.0% Cu 时, η - Cu_6Sn_5 相具有 {0001} 面的择优取向, 而当掺杂 3.0% 或 4.0% Cu 时, 择优取向转变为 {010} 面。此外, ε - Cu_3Sn 相仅存在 {0001} 和 $\{10\bar{1}0\}$ 面。高 Cu 含量有助于增加低角度晶界的数量, 提高残余应变、抗拉强度和显微硬度。

关键词: 无铅焊料; Sn–Cu 合金; 结晶取向; 显微组织; 金属间化合物; 力学性能

(Edited by Xiang-qun LI)